Nano Research

Open Access

Research Article

A Rh complex anchored cathode for cofactor regeneration and asymmetric reduction coupled with immobilized enzymes

Yaoxuan Li[1], Quan Yuan[1], Hao Zhao[1], Guanhua Liu[1,2] ✉, Xiaoyang Yue[1], Yunting Liu[1,2], and Yanjun Jiang[1,2] ✉

[1] *School of Chemical Engineering and Technology, Hebei University of Technology, Tianjin 300401, China*
[2] *National-Local Joint Engineering Laboratory for Energy Conservation in Chemical Process Integration and Resources Utilization, Hebei University of Technology, Tianjin 300130, China*

Cite this article: *Nano Research*, **2026**, *19*, 94907911. https://doi.org/10.26599/NR.2025.94907911

ABSTRACT: Chiral compounds have a huge market demand in the fields of pharmaceuticals, pesticides, and fine chemicals. Enzymatic electrosynthesis can couple enzyme catalysis, possessing high product purity, high efficiency, and mild conditions, with electrochemical regeneration of expensive cofactor nicotinamide adenine dinucleotide (NADH), possessing easy process monitoring and simple operation for efficient chiral synthesis. In this study, hydrophobic covalent organic framework (COF) was synthesized as the immobilized carrier, which not only enhanced the enzyme catalysis through enriching substrate but also enhanced the stability and reuse of the enzyme. Besides, Rh complex was anchored on hydrophilically-modified electrode to promote the regeneration of NADH, where the anchor of Rh complex can effectively avoid the mutual deactivation from the interference between electron mediator and enzyme, and simplify the separation of products. The immobilized enzyme catalysis and the electrochemical cofactor regeneration were coupled to construct an enzymatic electrosynthesis system for the efficient asymmetric reduction to obtain chiral alcohols, with a maximum turnover frequency (TOF) of 101.1 h^{-1}. Furthermore, the relevant parameters of the system were optimized, and the substrate scope was expanded.

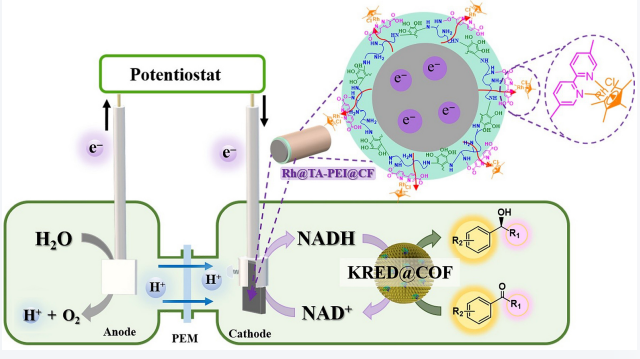

KEYWORDS: enzymatic electrosynthesis, asymmetric reduction, immobilized enzyme, nicotinamide adenine dinucleotide (NADH) regeneration, electron mediator

1 Introduction

Chiral compounds have a huge market demand in the fields of medicine, pesticides, and fine chemicals, among which chiral alcohols are the main building blocks for the production of active intermediates, thus receiving more and more attention [1]. The asymmetric synthesis of chiral alcohols can be mainly classified into metal catalysis, organic small molecule catalysis, and enzyme catalysis [2]. Compared with the other two methods, enzyme catalysis has high efficiency and product purity, under mild conditions in aqueous media [3, 4]. Asymmetric reduction of prochiral ketones catalyzed by ketoreductase (KRED) is an effective method for the synthesis of chiral alcohols, and has been increasingly paid attention to [5, 6]. At present, several industrial-scale KRED-based processes have been developed as a key step in asymmetric synthesis of blockbuster drugs, for example, atorvastatin (Lipitor), etc. [7, 8].

However, most enzymatic redox reactions usually cost stoichiometric cofactor, like nicotinamide adenine dinucleotide (phosphate) (NAD(P)H), which is necessary for the electron and proton transfer in the redox of substrates, but very expensive [9]. Therefore, developing efficient methods for NAD(P)H regeneration is urgent [10]. There are various methods for NAD(P)H regeneration, including biological, enzymatic, chemical, photochemical, electrochemical, and other methods [11]. Electrochemical method has the advantages of simple operation, low cost, easy process monitoring, and easy product separation, and has been considered to provide the cheapest reducing equivalents [12, 13]. In addition, electrical energy can be obtained from green and sustainable resources, which is an ideal energy system for human beings. Therefore, the coupling of electrochemical cofactor

Received: May 6, 2025; **Revised:** August 7, 2025
Accepted: August 12, 2025

✉Address correspondence to Guanhua Liu, ghliu@hebut.edu.cn; Yanjun Jiang, yanjunjiang@hebut.edu.cn

regeneration and enzyme catalysis has been increasingly focused on asymmetric synthesis [14]. Electron mediators are needed to overcome the poor selectivity, generation of undesired inactive dimers, and high overpotential during electrochemical cofactor regeneration [10]. As an artificial electron mediator, rhodium complex ([Cp*Rh(bpy)H_2O], abbreviated as **M** or Rh(III), where Cp* = pentamethylcyclopentadienyl, bpy = 2,2'-bipyridine) has gradually attracted attention in recent years, which is attributed to its high regeneration efficiency, selectivity, and stability. However, similar to other electron mediators, the homogeneous **M** is toxic and will cause the inactivation of enzyme [15, 16]. The immobilization of electron mediator on the electrode can inhibit the toxic effect on enzyme, simplify the separation of product, and realize the recycling and reuse of the electron mediator, thereby promoting the application of electrocatalytic cofactor regeneration. Zhang et al. [17] combined the two parts by covalently immobilizing the Rh complex on a Bucky paper electrode to make an NADH regeneration layer and coating the immobilized enzyme on the electrode to obtain an enzymatic substrate reduction layer. Lee et al. [18] synthesized graphene-**M** with three-dimensional structures via π–π and π–cation interaction hydrogels that can efficiently regenerate NADH for electroenzymatic reactions. Besides, free enzymes are poorly stable and difficult to recover and reuse, and the precursors for chiral alcohols are usually less water-soluble [19, 20]. The design and selection of a suitable immobilized enzyme carrier can not only improve the stability and reusability of the enzyme, but also enrich substrate, and thus catalytic efficiency can be enhanced. As an organic porous material with abundant functional groups, high specific surface area, and regular pore channels, covalent organic framework (COF) can effectively realize the immobilization of enzymes [21]. The enzymes can be immobilized on COF by covalent bonds, achieving high stability. What's more, hydrophobic groups can be introduced into COF, leading to increasing hydrophobic effects, which can enrich substrates and promote the local substrate concentration near the immobilized enzyme, thus the enzyme's catalytic efficiency can be improved.

Herein, an asymmetric reduction system was constructed by coupling the electrochemical cofactor regeneration system with the immobilized enzyme for the efficient production of chiral alcohols (Scheme 1). In the electrochemical cofactor regeneration part: A hydrophilic surface was formed on the carbon felt (CF) electrode by coating tannic acid (TA) and polyethyleneimine (PEI). This modification can increase the effective soaking surface of the electrode and enhance its electrochemical performance in aqueous solution, because the pristine CF is highly hydrophobic. Furthermore, the modification increased available functional groups that can be used for further covalent immobilization of the electron mediator **M**. In the catalytic part, by immobilized enzyme: COF with hydrophobic property was chosen as the carrier for the immobilization of enzyme, which can enrich substrate around the enzyme catalyst and improve the catalytic efficiency. Finally, the amount of initial NADH and KRED@COF was optimized to realize the efficient asymmetric synthesis of chiral alcohols, and the substrate scope was then expanded. The maximum turnover frequency (TOF) of reaction reached 101.1 h^{-1}.

2 Experimental section

2.1 Preparation of COF

COF was prepared according to the method in reference [21]. 1,3,5-tri-(4-aminophenyl)benzene (TAPB, 0.04 mmol) and 2,5-dimethoxyterephthalaldehyde (DMTA, 0.06 mmol) (or TAPB (0.02 mmol) and 2,5-dihydroxyterephthalaldehyde (DHTP, 0.03 mmol) for COF–OH) were added to a centrifugation tube containing acetonitrile for ultrasonic dissolution. Then acetic acid (12 M) was added under stirring. After turning milky yellow, the

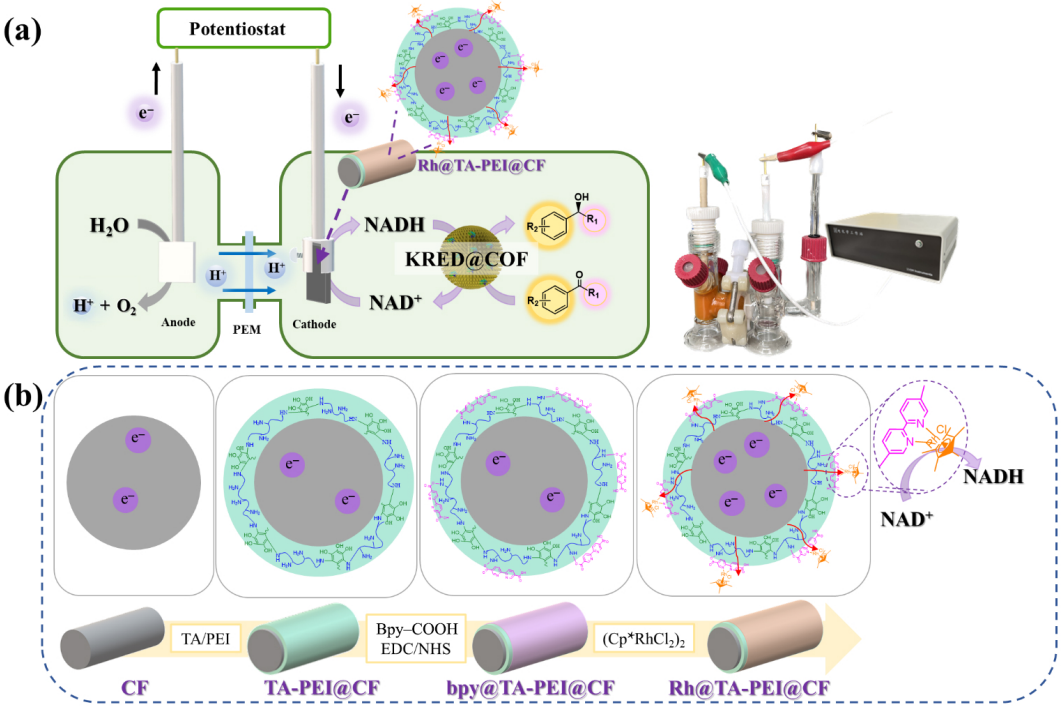

Scheme 1 (a) Schematic diagram of electroenzymatic system for asymmetric chiral alcohol synthesis. (b) Schematic diagram of Rh@TA-PEI@CF cathode for NADH regeneration.

mixture was left to stand at room temperature for 5 days. The precipitate was washed three times with tetrahydrofuran and ethanol, and the obtained COF was extracted in tetrahydrofuran solution for 12 h by Soxhlet and then dried under vacuum at 60 °C for 12 h. If it is not specially marked as COF–OH, the COF in the following text refers to COF-methoxy (OMe).

2.2 Preparation of KRED@COF

10 mg COF was added to a centrifuge tube and activated with glutaraldehyde solution with concentration gradients. After a certain period, the glutaraldehyde was removed by centrifugation. Then the COF was washed with 0.1 M phosphate buffered saline (PBS, pH = 6) and ethanol twice, dried under vacuum at 60 °C for 12 h. The activated COF was dispersed in PBS solution with ultrasonication, followed by adding enzyme and incubating in a shaker for a period of time. After centrifuging, the precipitate was washed with PBS and freeze-dried to obtain KRED@COF.

2.3 Synthesis of free Rh complex

The **M**, Cp*Rh(2,2'-bipyridyl-5,5'-dicarboxylic)Cl_2, was synthesized routinely and detailed in the Electronic Supplementary Material (ESM) [22].

2.4 Preparation of Rh@TA-PEI@CF electrode

The detailed steps for electrode preparation are shown in Scheme 1(b). CF with 1.0 cm × 2.0 cm was cleaned with pure water to remove surface impurities, and soaked in a mixed solution of TA and PEI at pH = 3, tuned by HCl, for 5 h, followed by adjusting to pH = 6.5 with NaOH. After further soaking for 10 min, the obtained TA-PEI@CF was rinsed with pure water. The above-prepared electrode was stirred in the mixture of 2,2'-bipyridine-5,5'-dicarboxylic and PBS (100 mM, pH = 6). Then 1-ethyl-3-(3-(dimethylamino) propyl)carbodiimide (EDC) and N-hydroxysuccinimide (NHS) were added and stirred for 48 h. Then the electrode was washed with water three times and added to $(Cp^*RhCl_2)_2$ PBS buffer solution for 24 h. Afterwards, the electrode was washed with water three times to remove excess free **M**. Finally, the obtained Rh@TA-PEI@CF was washed with water three times.

2.5 Electrochemical NADH regeneration

Electrochemical NADH regeneration was performed in a three-electrode system with an H-cell containing two compartments separated by a proton exchange membrane (PEM, Nafion N-117) on electrochemical analyzer CHI600E. The Rh@TA-PEI@CF electrode was used as the working electrode with Ag/AgCl (3.5 M KCl) as reference electrode and platinum sheet as counter electrode. Pure water and PBS buffer (0.1 M, pH = 6) were added to the anode cell and cathode cell, respectively. Before electrochemical catalysis, N_2 was bubbled in the cathode cell for 30 min to prevent NADH oxidation. Cyclic voltammetry (CV) curves were determined in the presence of NAD^+ at a scan rate of 50 mV/s from −0.4 to −1.2 V (vs. Ag/AgCl). The regeneration of NADH from NAD^+ was realized by electrocatalysis using the Rh@TA-PEI@CF electrode at a constant voltage of −0.8 V (vs. Ag/AgCl). NADH regeneration is detected by adding a 200 μL sample to a 96-well plate and reading the absorbance at 340 nm by microplate reader, and the standard curve of NADH can be found in Fig. S1 in the ESM.

2.6 Bioelectrochemical asymmetric synthesis

The bioelectrocatalysis for asymmetric synthesis is carried out in the three-electrode system as shown in Scheme 1(a). 10 mL water is added to the anode cell, and protons are generated by electrolysis of water, followed by transportation to the cathode cell through PEM. 10 mL of PBS (100 mM, pH = 6) was added to the cathode cell with KRED@COF and a certain amount of NADH and substrate. The electroenzymatic asymmetric reduction occurs in the cathode cell at a constant potential of −0.8 V vs. Ag/AgCl and stirring of 800 rpm. The reaction solution was extracted with ethyl acetate three times, then rotary distillation, and filtered through a needle filter (0.22 μm) to remove the insoluble impurities. The enantiomeric excess (*ee*) value was calculated by Eq. (S1) in the ESM.

3 Results and discussion

3.1 Molecular docking simulations

Molecular simulation was carried out to clarify the reduction mechanism of 2-chloroacetophenone by *Lactobacillus fermentum* short-chain dehydrogenase/reductase 1 (*Lf*SDR1) (KRED) [23] (Fig. 1). The short-chain dehydrogenase typically follows a sequential catalytic mechanism as follows: Firstly, the NADH will be attached by the Rossman fold structure in the active pocket of enzyme, followed by substrate, which will be activated by catalytic residues tyrosine 152 (Y152) and attacked by the C4-proton of NADH to generate the chiral alcohol. In this catalytic process, the solubility of substrate in aqueous phase and the attack of NADH on the activated ketone are the decisive steps [24]. Moreover, the enzyme is covalently immobilized on COF-Ome, whose hydrophobic methoxy group provides an enrichment effect for the substrates, accelerating the activation of the substrate molecules in the active pocket and leading to an enhanced catalytic performance of the enzyme-catalyzed reaction [25, 26].

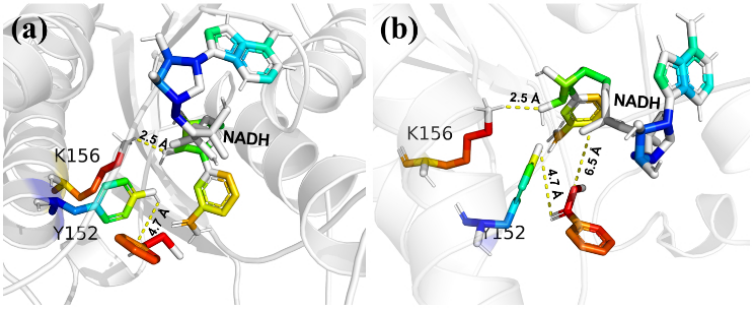

Figure 1 Molecular docking simulations for the catalysis mechanism of KRED@COF. (a) Fixation and activation of NADH and 2-chloroacetophenone by amino acids lysine 156 (K156) and Y152. (b) The relative distance between the cofactor and the activated substrate.

3.2 The immobilization of enzyme

The sodium dodecyl sulfate-polyacrylamide gel electrophoresis (SDS-PAGE) image demonstrated the successful purification of KRED(*Lf*SDR1) (Fig. S2 in the ESM). As shown in Fig. S3 in the ESM, firstly, a hollow spherical COF with high stability was prepared using the Ostwald ripening method according to our previous research [21], then KRED@COF was prepared. The scanning electron microscope (SEM, Fig. 2(a)) and transmission electron microscope (TEM, Fig. 2(b)) images show that the COF is a well-dispersed hollow sphere with a rough flower-like structure and diameter of 600–800 nm, as well as the connection of the inner cavity to the outside via through-holes. The X-ray diffraction (XRD) patterns (Fig. 2(c)) reveal that the COF has distinct diffraction peaks at (100), (110), (200), (210), and (220), respectively [21]. The pore structures and specific surface areas of COF, glutaraldehyde-activated COF (COF-GA), and KRED@COF were characterized by N_2 adsorption–desorption. As shown in Fig. 2(d), Brunauer–Emmett–Teller (BET) and Barrett–Joyner–Halenda (BJH) analysis show that all samples belong to the Langmuir IV isotherm, and the hysteresis loop is H1 type (relative pressure (P/P_0) > 0.4), indicating that the material is a spherical mesoporous material with relatively uniform size. As shown in Table S1 in the ESM, the specific surface area and pore volume of COF were 2195 m^2/g and 1.70 cm^3/g, respectively, which successively decreased for COF-GA and KRED@COF, demonstrating the successful activation of GA and the successful loading of KRED on COF. In addition, according to the pore size distribution diagram (Fig. S4 and Table S1 in the ESM), the average pore diameter of COF, COF-GA, and KRED@COF decreases in sequence, which proves that the activation of COF by GA and the loading of KRED blocks part of the pores, resulting in a decrease in the average pore size. In addition, the hydrophilicity of COF was studied using COF–OH for comparison with COF-OMe. As shown in Fig. 2(e), the water contact angle (WCA) of COF–OH is lower due to the higher hydrophilicity of –OH.

After immobilization of enzyme, the diffraction peaks of KRED@COF do not change much and retain obvious crystal structure, but the peak intensity of COF is slightly decreased. As shown in the Fourier transform infrared (FT-IR) spectra (Fig. 2(f)), the characteristic peaks of COF appear at 1614, 1284, and 1461 cm^{-1}, respectively, which are caused by the stretching vibration of C=N and C–O and the bending vibration of $–CH_3$. The characteristic peak at 1665 cm^{-1} is caused by C–O stretching vibration in the amide I band [27], which can be seen in the FT-IR spectrum of KRED. A distinct peak of the amide bond can also be seen on KRED@COF, demonstrating the successful immobilization of KRED. As shown in the mechanical stability test (Fig. S5 in the ESM), after 24 h of mechanical stirring, free KRED retains only 10% of the initial enzyme activity, while KRED@COF can still retain 70% of the initial enzyme activity. The secondary structure of enzyme was analyzed by circular dichroism (CD) spectra to determine the conformation change. As shown in Fig. 2(g), free KRED shows two similar negative cotton peaks near 210 and 220 nm subject to stirring, formed by the mixing of multiple secondary structures. A small amount of protein precipitation was observed using free KRED, resulting in a decrease in protein amount. Comparatively, there is no significant difference in the protein secondary structure of KRED@COF after stirring, indicating that the damage of mechanical stirring to enzyme is heavily inhibited, indicating the protection of COF on enzyme. In addition, the peak positions of free KRED and KRED@COF are similar, indicating that COF maintains the original secondary structure of KRED in the process of immobilization. The secondary structure of proteins depends on the ordered arrangement of peptide bonds, which are mainly maintained by intermolecular hydrogen bonds [28], so the change of intermolecular interaction will affect the secondary structure of proteins. The CD spectrum of free KRED has an obvious negative peak at 210–230 nm and a positive absorption peak near 195 nm, which are mainly α-helix and β-sheet structural characteristic regions, indicating the main secondary structures of free KRED. The fitting results (Fig. 2(h)) show the relative content of α-helix and β-sheet in the free KRED, which accounts for 60.6% of the whole secondary structure. α-helix and β-sheet are the key structures to maintain the hydrogen bond of protein. The high content of α-helix and β-sheet indicates a relatively stable spatial structure. However, the negative absorption peak of free KRED decreases after stirring, and the positive

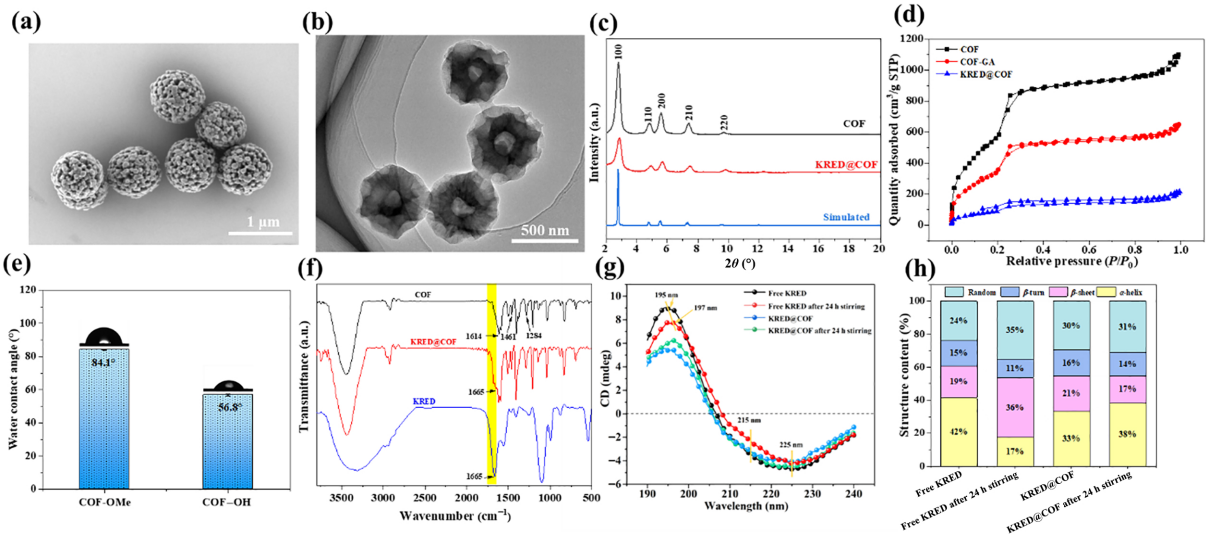

Figure 2 (a) SEM and (b) TEM of COF. (c) XRD patterns of COF and KRED@COF. (d) Nitrogen adsorption–desorption isotherms of COF, COF-GA, and KRED@COF. (e) WCAs of COF-OMe and COF–OH. (f) FT-IR spectra of COF, KRED@COF, and KRED. (g) CD spectra and (h) relative content of protein secondary structure of free KRED, free KRED after 24 h stirring, KRED@COF, and KRED@COF after 24 h stirring.

absorption peak decreases with shifting to 197 nm. The relative contents of α-helix, β-sheet, and Random all change. These data indicate that mechanical stirring highly interferes with the secondary structure of free KRED, and the α-helix of protein is transformed into β-sheet and Random, which may also affect KRED function. The fitting results show that the relative contents of α-helix and β-sheet of KRED@COF did not change significantly after stirring, with only a slight decrease in the positive peak at 195 nm and the negative peak at 225 nm. The fitting results also show that α-helix and β-sheet of the KRED@COF transformed slightly after stirring, and the relative contents of β-turn and Random remained steady, indicating that the KRED@COF has high structural stability under mechanical stirring.

As shown in Fig. S6(a) in the ESM and standard curves for protein (Fig. S1 in the ESM), the amount of KRED immobilized by COF increases with GA concentration. Similarly, when GA concentration increases from 0.5 wt.% to 2.5 wt.%, the enzyme activity of KRED@COF increases with the maximum enzyme activity of 110.9 U/$g_{support}$ (U = enzyme units, U/$g_{support}$ stands for units per gram of support). With the increase of GA concentration, the –CHO covalently bound to enzyme molecules increases, leading to higher enzyme protein loading and apparent enzyme activity. When GA concentration further increases to 3.0 wt.%, the enzyme loading amount continues to increase, but the enzyme activity decreases, and the reason is that the active sites of enzyme molecules cover each other with excess enzyme loading, resulting in a decrease in apparent activity. Therefore, 2.5 wt.% GA was determined as the optimal concentration. As shown in Fig. S6(b) in the ESM, the equilibrium time for GA activation was 1.5 h.

The substrate adsorption ability of KRED@COF-OMe and KRED@COF–OH catalysts is compared (Fig. S7 in the ESM). The results show that KRED@COF-OMe has larger substrate adsorption than KRED@COF–OH due to the hydrophobic groups on the pore surface. The carrier with hydrophobic microenvironment can provide a suitable reaction microenvironment for ketoreductase enzymes [29]. The substrate is enriched around the carrier through capillary action and hydrophobic action, which can increase the concentration of substrate near the enzyme molecules, thus speeding up the reaction and promoting the forward reaction [30]. Therefore, KRED@COF-OMe is mainly focused on this study.

3.3 Fabrication of Rh@TA-PEI@CF electrode

Firstly, by modifying a layer of hydrophilic groups with $–NH_2$ on the surface of CF, and then using the covalent reaction of $–NH_2$ with bpy–COOH to graft bpy to the electrode surface, and then complexing Rh to form a modified electrode with anchored electron mediator **M**. Figures 3(a) and 3(b) show the SEM image of Rh@TA-PEI@CF and the corresponding distribution of C, N, O, and Rh elements in energy-dispersive X-ray (EDX) elemental mapping images. Accordingly, Rh element is uniformly dispersed on the CF electrode, which proves the successful loading of **M**. As shown in the cross-section images (Fig. 3(c) and Fig. S8 in the

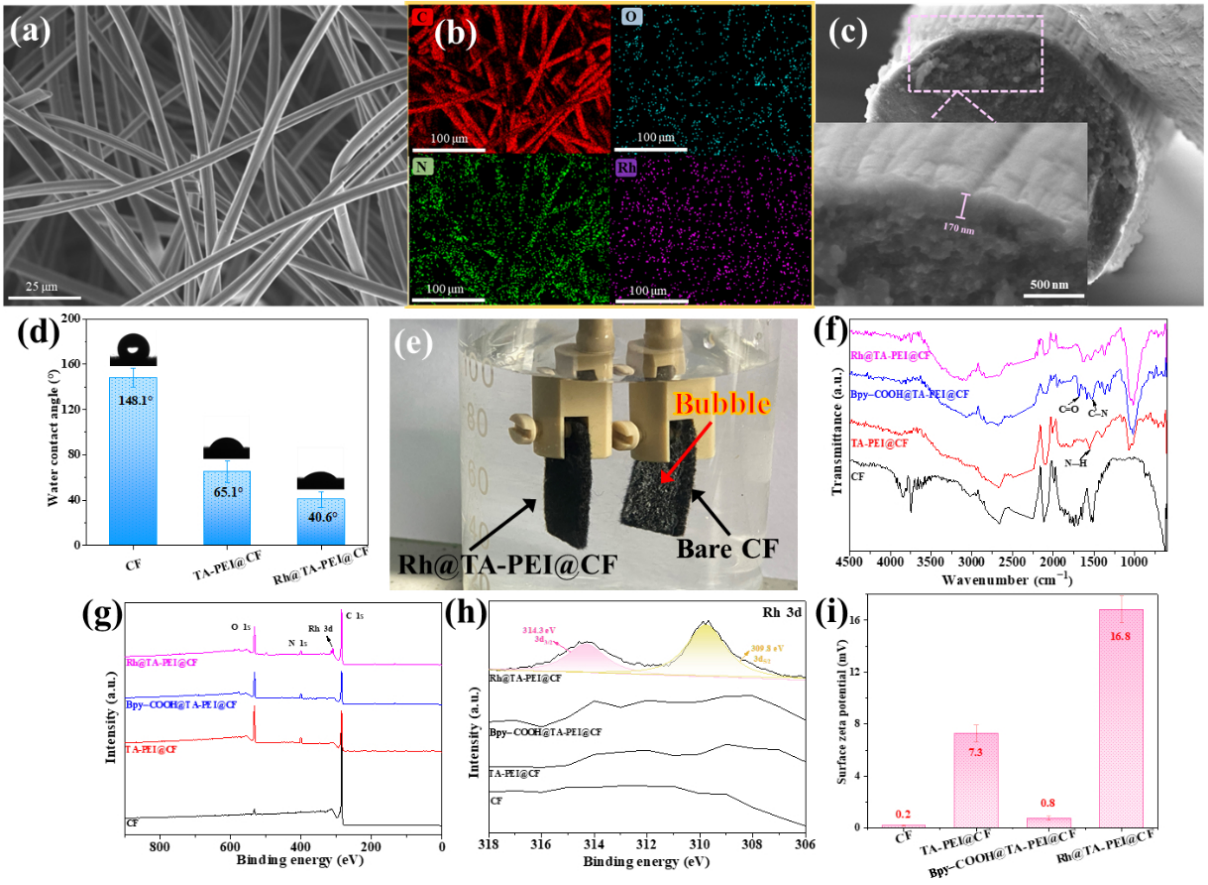

Figure 3 (a) SEM and (b) EDX elemental mapping of Rh@TA-PEI@CF. (c) SEM and magnification of Rh@TA-PEI@CF cross-section. (d) WCAs of CF, TA-PEI@CF, and Rh@TA-PEI@CF. (e) Comparison of hydrophobicity between Rh@TA-PEI@CF and bare CF. (f) FT-IR spectra of CF, TA-PEI@CF, bpy–COOH@TA-PEI@CF, and Rh@TA-PEI@CF. ((g) and (h)) XPS survey spectra of CF, TA-PEI@CF, bpy–COOH@TA-PEI@CF, and Rh@TA-PEI@CF with (g) XPS wide scan spectra and (h) high-resolution spectra of Rh 3d. (i) Surface zeta potential of CF, TA-PEI@CF, bpy–COOH@TA-PEI@CF, and Rh@TA-PEI@CF.

ESM), the CF surface was very rough after coating TA-PEI and **M**, forming a layer of ~ 170 nm on the surface. In PBS (pH = 6.0), the TA-PEI@CF can still maintain stability. Due to the increased roughness of CF surface and the addition of hydrophilic groups $-NH_2$ through surface modification, CF can be sufficiently infiltrated in solution, which can be confirmed by the characterization of WCA (Figs. 3(d) and 3(e)).

As shown in FT-IR spectra of the electrodes (Fig. 3(f)), the characteristic peak of TA-PEI@CF at 1552 cm^{-1} is caused by the bending vibration of N–H, indicating the successful coating of TA-PEI on CF. The characteristic peaks of bpy–COOH@TA-PEI@CF at 1539 and 1689 cm^{-1} are caused by the stretching vibrations of C=N and C=O bonds, respectively, which indicate the successful grafting of bpy–COOH by reaction with $-NH_2$.

The chemical state of the elements in the electrodes was elucidated by X-ray photoelectron spectroscopy (XPS) analysis. As shown in Fig. 3(g), a new Rh 3d binding energy peak appears in Rh@TA-PEI@CF after the coordination of **M**. In Fig. 3(h), the high-resolution Rh 3d spectra have two peaks at 309.8 and 314.3 eV, corresponding to Rh $3d_{5/2}$ and Rh $3d_{3/2}$, demonstrating the successful coordination of Rh complex with bpy. The high-resolution C 1s spectra have three peaks at around 286.1, 288.7, and 291.3 eV attributed to C–N, C–O, and N–C=N, respectively (Fig. S9(a) in the ESM). The peaks in high-resolution N 1s spectra (Fig. S9(b) in the ESM) at around 399.6 and 401.7 eV are attributed to C–N=C and C–NH_2, respectively. The peaks in high-resolution O 1s spectra (Fig. S9(c) in the ESM) at 531.7 and 533.0 eV are ascribed to C–O and C=O, respectively.

The abundant $-NH_2$ on TA-PEI@CF surface increases zeta potential of the electrode (Fig. 3(i)), which is decreased by the grafted bpy–COOH for bpy–COOH@TA-PEI@CF electrode. **M** has much positive charge, so the coordination of **M** to bpy increases the overall charge of Rh@TA-PEI@CF. The above characterization demonstrates the successful coating of TA-PEI, grafting of bpy–COOH, and coordination of **M**.

We used the electrodes as cathode for NADH regeneration. The unmodified bare CF has no redox peak in NAD^+ solution, while the Rh-modified Rh@TA-PEI@CF has a clear reduction peak at ~ −0.8 V (vs. Ag/AgCl) (Fig. 4(a)). Therefore, −0.8 V (vs. Ag/AgCl) was chosen as the best reduction potential for NADH regeneration. The electrochemical impedance spectroscopy (EIS) plots in Fig. 4(b) show that the impedance is very high for hydrophobic bare CF. However, when the TA-PEI surface layer is modified, the impedance decreases, because the solution of the electrochemical system could rapidly penetrate into TA-PEI@CF electrode due to the increased CF surface roughness and the addition of more hydrophilic groups $-NH_2$, which increases the overall surface area of the electrode for the mass transfer. When loaded with **M**, Rh@TA-PEI@CF shows a further decrease in the impedance of the electrode due to its additional loading of metal substances, showing the enhancement of electrochemical behavior. This high hydrophilicity and surface roughness increase the effective surface area of the electrode during NADH regeneration, promote electron and mass transfer between the cathode and electrolyte, and thus increase the regeneration efficiency of NADH, which can be verified by CV (Fig. 4(a)) and EIS Nyquist plots (Fig. 4(b)) [31–33]. The reaction solutions in the NADH regeneration cell were measured using a ultraviolet (UV) spectrophotometer at full wavelengths. As shown in Fig. 4(c), the concentration of NADH increases with time, and the peaks are higher.

To ensure the efficient regeneration of NADH, the chemical structure of CF surface coating material was optimized by changing the ratio of [TA]/[PEI] concentration, amidation coupling reaction time, and bpy–COOH concentration to investigate their effects on NADH regeneration efficiency.

The NADH regeneration of Rh@TA-PEI@CF samples with

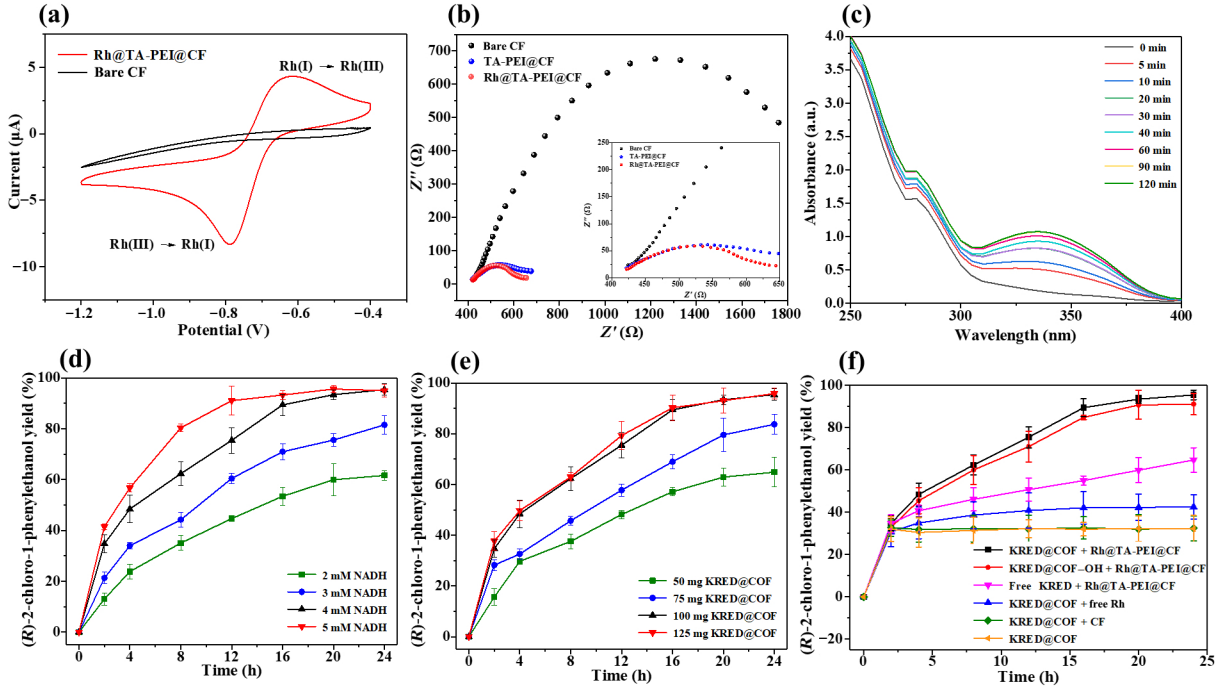

Figure 4 (a) CV curves of the bare CF and Rh@TA-PEI@CF in the presence of 2 mM NAD^+ when the scan rate is 10 mV/s. (b) EIS Nyquist plots of bare CF, TA-PEI@CF, and Rh@TA-PEI@CF in 0.1 M PBS (pH 6.0) containing 5.0 mM of $[Fe(CN)_6]^{3-/4-}$ and 0.1 M KCl at a scan rate of 5 mV/s. (c) UV–vis spectra of electrochemical regeneration of NADH. (d) Reaction process curves with different initial NADH addition amounts. (e) Reaction process curves with different initial KRED@COF addition amounts. (f) Reaction process curves of various reaction systems with an external voltage of −0.8 V (vs. Ag/AgCl) (100 mg KRED@COF and 4 mM NADH).

different [TA]/[PEI] ratios gradually increases with the extension of time (Fig. S10(a) in the ESM). As the PEI content increases with [TA]:[PEI] ratio from 1:5 to 1:20, the NADH regeneration increases from 110 to 285 μM. This may be attributed to the increase in Rh content detected by the inductively coupled plasma optical emission spectrometry (ICP-OES) spectrometer (Fig. S10(c) in the ESM). Subsequently, with the increase of [PEI] at the [TA]:[PEI] ratio from 1:20 to 1:30, the NADH regeneration decreases slightly. The Rh content detected by ICP-OES decreases (Fig. S10(c) in the ESM). The electrochemical signals during NADH regeneration (Fig. S10(b) in the ESM) are the strongest at the [TA]/[PEI] ratio of 1/20, which indicates that the main factor affecting the regeneration performance of NADH is the content of Rh grafting.

Extending the –COOH activation time and amidation reaction time is beneficial to improve the efficiency of electrochemical NADH regeneration (Fig. S11(a) in the ESM). The regeneration efficiency of NADH did not continue to increase after 48 h, indicating that the amidation reaction between the amino and carboxyl groups was completed, which was verified by the electrochemical *i*–*t* signals in Fig. S11(b) in the ESM.

As shown in Fig. S12(a) in the ESM, the maximum NADH regeneration amount of Rh@TA-PEI@CF gradually increases from 185 to 300 μM as the bpy–COOH concentration increases from 5 to 20 mM, which may be attributed to the increase in Rh content from 1.160 to 1.516 μg/cm^2 as detected by ICP-OES (Fig. S12(c) in the ESM). With further increasing the bpy–COOH concentration to 30 mM, the NADH regeneration amount decreases slightly, although the Rh content detected by ICP-OES increases, which may be due to the superposition of **M** active sites, leading to a decrease in the regeneration efficiency of NADH. Moreover, the electrochemical signal is the strongest at bpy–COOH concentration of 20 mM (Fig. S12(b) in the ESM), which is consistent with the results of NADH regeneration.

The solution in the cathode cell before and after the NADH regeneration reaction is lyophilized and subjected to nuclear magnetic resonance (NMR) analysis, which proves the successful regeneration of NADH (Fig. S13 in the ESM).

3.4 Electroenzymatic asymmetric chiral alcohol synthesis

The enzyme-catalyzed asymmetric chiral alcohol synthesis system was coupled with the electrochemical cofactor regeneration system. As shown in Fig. 4(d), with the extension of reaction time, the (*R*)-2-chloro-1-phenylethanol yield continues to increase. The faster reaction rate in the first 4 h is mainly due to a rapid positive push from the added NADH. With the extension of time, the increase in yield becomes slower, and the electrochemically regenerated NADH promotes the reaction. At initial NADH addition amount of 4 mM, the (*R*)-2-chloro-1-phenylethanol yield reached > 95% at 24 h, which is obviously higher than the yield of 61.6% with NADH addition amount of 2 mM, indicating the effectiveness of electrochemical NADH regeneration. Further increase of the NADH addition amount does not increase the final yield. These results indicate that the addition of NADH at higher concentrations could not promote the regeneration process of NADH. The earlier arrival of > 95% yield is due to the addition of high initial NADH concentrations. Considering the high price of NADH, it is more meaningful to use regenerated NADH for enzyme catalysis, so the addition amount of 4 mM NADH was selected.

The addition amount of immobilized enzyme was optimized to match the electrochemical regeneration system. As shown in Fig. 4(e), the coupled system can achieve > 95% yield at both 100 and 125 mg KRED@COF. The excess addition of KRED@COF does not increase the reaction rate; the rate-limiting step at this point is the regeneration of NADH. Therefore, 100 mg of KRED@COF was chosen as the optimal immobilized enzyme addition amount.

In the whole reaction, the electron mediator Rh(III) first acquires two e^- and one H^+ on the electrode, becoming RhH in the reducing state. RhH then reacts with NAD^+, where NAD^+ regenerates into NADH while RhH loses e^- and H^+ returns to its oxidation state. The regenerated NADH and the substrate are catalyzed by enzyme to produce the product and NAD^+, which re-enters the cycle. The main reactions are as follows

$$\mathrm{Rh(III)} + \mathrm{e^-} + \mathrm{H^+} \rightarrow \mathrm{RhH} \quad (1)$$

$$\mathrm{RhH} + \mathrm{NAD^+} + \mathrm{e^-} \rightarrow \mathrm{Rh(III)} + \mathrm{NADH} \quad (2)$$

$$\mathrm{Ketone} + \mathrm{NADH} \xrightarrow{\mathrm{Enzyme}} \mathrm{Alcohol} + \mathrm{NAD^+} \quad (3)$$

To further highlight the advantages of the present electroenzymatic synthesis system, a comparison was carried out using the model reduction reaction of 2-chloroacetophenone to (*R*)-2-chloro-1-phenylethanol (Fig. 4(f)). The product yield is only 32% using bare CF electrode for cofactor regeneration, indicating the poor regeneration ability of the bare CF electrode. When free **M** complex with equal Rh amount to Rh@TA-PEI@CF is added for cofactor regeneration, the product yield is only 42.5%, indicating the free-state electron mediator has poor ability in enhancing the electron transfer for NADH regeneration. The product yield is 3 and 2.25 times that of the above two systems, respectively, using the Rh@TA-PEI@CF cathode. The reason is that the fixation of **M** on electrode is more effective than dispersing it in solution as free state to transfer electrons: Firstly, the modification of electron mediator on bare electrode can decrease impedance and enhance electrochemical property, which makes the electrode more efficient in electron transfer and NADH regeneration. Secondly, **M** has a toxic effect on enzyme, which makes the two modules affect each other, leading to a decrease in enzyme activity. Besides, fixing electron mediator on electrode is conducive to the recovery of the precious metal Rh and facilitates subsequent product separation and purification. In addition, we compared three more enzyme catalysts, i.e., free KRED, KRED@COF–OH, and KRED@COF, in the electroenzymatic reduction of prochiral ketone. The free KRED is seriously deactivated due to the poor mechanical stability of free enzyme under stirring (Fig. S5 in the ESM), and the yield is only about 65%. In order to endow the enzyme with high stability and recovery, COF was selected as the carrier to immobilize enzyme. Considering two COFs, the (*R*)-2-chloro-1-phenylethanol yield using COF-OMe carrier with hydrophobic groups is 4.3% higher than that of hydrophilic COF–OH carrier. Because hydrophobic group OMe can enrich the substrate and increase the local substrate concentration around enzyme molecules, thereby improving the catalytic efficiency, as indicated in Fig. 2(e) and Fig. S7 in the ESM.

The TOF of NADH based on the reduction reaction center **M** is calculated by using Eq. (4)

$$\mathrm{TOF} = \frac{\text{Amounts of product molecules}}{\text{Amounts of mediator} \times \text{reaction time}} = \frac{C_{\mathrm{NADH}}}{C_{\mathbf{M}} t} \quad (4)$$

where C_{NADH} and $C_{\mathbf{M}}$ denote the concentration of regenerated

NADH and **M**. According to the equation, the maximum TOF of the reaction was calculated to be 101.1 h^{-1}, which is higher than most reported NADH regeneration systems (Table 1).

In order to verify the universality of the present electroenzymatic synthesis system, we extended the substrate scope. As shown in Fig. 5, higher than 81% yield and 94% *ee* value can be obtained for the ten products. Due to the different affinity between substrate and enzyme, the yield of different substrates catalyzed by enzyme is also different [43].

4 Conclusions

In this study, we constructed an electroenzymatic synthesis system for the efficient production of chiral alcohols by using an immobilized enzyme catalyst in combination with an **M** fixed hydrophilically-modified CF electrode. The COF carrier enriches substrate and enhances the performance and stability of enzyme. Using Rh@TA-PEI@CF electrode for cofactor regeneration, the yield is 3 and 2.25 times that of using bare CF electrode and free **M**, respectively. The relevant parameters of the electroenzymatic synthesis process were optimized, and the maximum TOF in the reaction is 101.1 h^{-1}, higher than most reported systems. The electroenzyme coupled system is efficient for various substrate scopes. The research is expected to provide prospects for the electroenzymatic synthesis of chiral compounds.

Electronic Supplementary Material: Supplementary material (chemicals and materials; characterization; experimental section; figures and tables; and ^{1}H and ^{13}C NMR spectra of the products recorded in $CDCl_3$) is available in the online version of this article at https://doi.org/10.26599/NR.2025.94907911.

Data availability

All data needed to support the conclusions in the paper are presented in the manuscript and the Electronic Supplementary Material. Additional data related to this paper may be requested from the corresponding author upon request.

Acknowledgements

This work was supported by the National Key Research and Development Program of China (No. 2023YFA0914500), the National Natural Science Foundation of China (Nos. 22378096, 22308083, and 22178083), the Natural Science Foundation of Hebei

Table 1 Comparison of NADH regeneration performance in different systems

System	Electron mediator	Catalyst	Product	TOF (h^{-1})	References
Electroenzymatic	Rh-complex	KRED@COF	*α*-chiral alcohol	101.1	This study
Electroenzymatic	Rh-complex	GDH	L-glutamate	~ 57	[18]
Electroenzymatic	Rh-complex	HbpA	*α*-substituted phenols	~ 11	[34]
Electroenzymatic	Rh-complex	FDH	Formic acid	1.64	[35]
Electroenzymatic	Rh-complex	D-sorbitol dehydrogenase/ galactitol dehydrogenase	D-sorbitol/1,2-propanediol	164	[36]
Electroenzymatic	Cholesterol-modified gold amalgam electrode	—	—	67	[37]
Electroenzymatic	NR	FDH@SBA-15	Formic acid	1.25	[38]
Electroenzymatic	MV^{2+}	nFDH@ZIF-90@CA	Formate	0.13	[39]
Photoenzymatic	Rh-complex	FDH	Formic acid	70.82	[40]
Photoenzymatic	Rh-complex	YADH	Methanol	46.8	[41]
Photoenzymatic	Rh-complex	ADH	Methanol	22.5	[42]

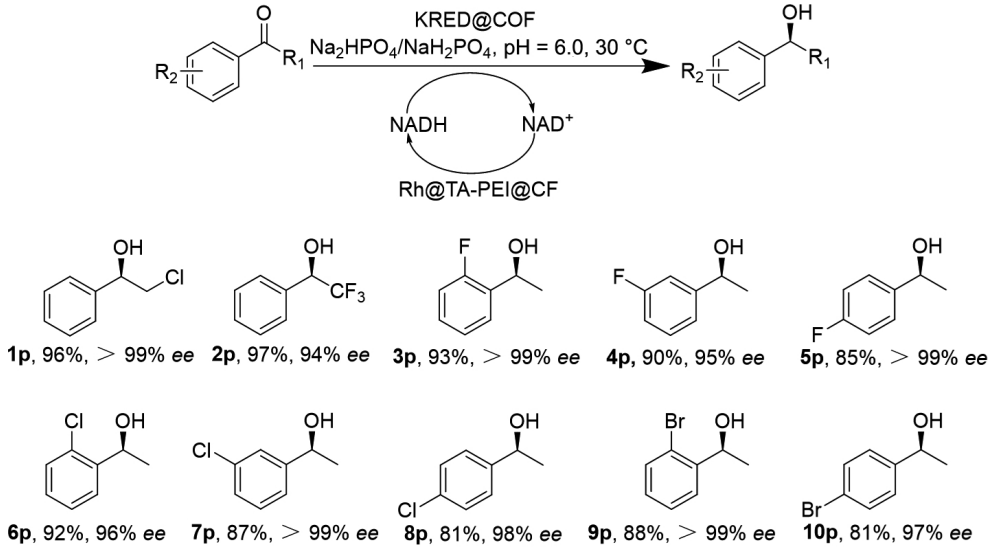

Figure 5 Electroenzymatic asymmetric synthesis of chiral alcohols.

Province (No. B2022202014), and the Educational Commission of Hebei Province (No. JZX2023012).

Declaration of competing interest

All the contributing authors report no conflict of interests in this work.

Author contribution statement

Y. X. L.: Conceptualization, methodology, formal analysis, data curation, writing – original draft. Q. Y.: Formal analysis, methodology. H. Z.: Visualization, investigation. G. H. L.: Conceptualization, funding acquisition, resources, supervision, writing – review & editing. X. Y. Y.: Software, validation. Y. T. L.: Visualization. Y. J. J.: Project administration, funding acquisition, resources, supervision, writing – review & editing. All the authors have approved the final manuscript.

Use of AI statement

None.

References

[1] Shanati, T.; Lockie, C.; Beloti, L.; Grogan, G.; Ansorge-Schumacher, M. B. Two enantiocomplementary ephedrine dehydrogenases from *Arthrobacter* sp. TS-15 with broad substrate specificity. *ACS Catal.* **2019**, *9*, 6202–6211.

[2] Gröger, H.; Wilken, J. The application of L-proline as an enzyme mimic and further new asymmetric syntheses using small organic molecules as chiral catalysts. *Angew. Chem., Int. Ed.* **2001**, *40*, 529–532.

[3] Kim, S.; Ga, S.; Bae, H.; Sluyter, R.; Konstantinov, K.; Shrestha, L. K.; Kim, Y. H.; Kim, J. H.; Ariga, K. Multidisciplinary approaches for enzyme biocatalysis in pharmaceuticals: Protein engineering, computational biology, and nanoarchitectonics. *EES Catal.* **2024**, *2*, 14–48.

[4] Choi, J. M.; Han, S. S.; Kim, H. S. Industrial applications of enzyme biocatalysis: Current status and future aspects. *Biotechnol. Adv.* **2015**, *33*, 1443–1454.

[5] de Gonzalo, G.; Paul, C. E. Recent trends in synthetic enzymatic cascades promoted by alcohol dehydrogenases. *Curr. Opin. Green Sustain. Chem.* **2021**, *32*, 100548.

[6] Yuan, Q.; Ma, L.; Kong, W. X.; Liu, J. Q.; Zhang, S. L.; Yan, J. J.; Bai, J.; He, Y.; Zhou, L. Y.; Liu, Y. T. et al. Enzymatic synthesis of chiral alcohols using ketoreductases. *Catal. Rev.* **2025**, *67*, 283–322.

[7] Yang, Z. Y.; Ye, W. J.; Xie, Y. Y.; Liu, Q. H.; Chen, R.; Wang, H. L.; Wei, D. Z. Efficient asymmetric synthesis of ethyl (*S*)-4-chloro-3-hydroxybutyrate using alcohol dehydrogenase *Sm*ADH31 with high tolerance of substrate and product in a monophasic aqueous system. *Org. Process Res. Dev.* **2020**, *24*, 1068–1076.

[8] Ying, X. X.; Zhang, J.; Wang, C.; Huang, M. J.; Ji, Y. T.; Cheng, F.; Yu, M. L.; Wang, Z.; Ying, M. R. Characterization of a carbonyl reductase from *Rhodococcus erythropolis* WZ010 and its variant Y54F for asymmetric synthesis of (*S*)-*N*-boc-3-hydroxypiperidine. *Molecules* **2018**, *23*, 3117.

[9] Monti, D.; Ottolina, G.; Carrea, G.; Riva, S. Redox reactions catalyzed by isolated enzymes. *Chem. Rev.* **2011**, *111*, 4111–4140.

[10] Li, Y. X.; Liu, G. H.; Kong, W. X.; Zhang, S. Q.; Bao, Y. M.; Zhao, H.; Wang, L. H.; Zhou, L. Y.; Jiang, Y. J. Electrocatalytic NAD(P)H regeneration for biosynthesis. *Green Chem. Eng.* **2024**, *5*, 1–15.

[11] Wang, X. D.; Saba, T.; Yiu, H. H. P.; Howe, R. F.; Anderson, J. A.; Shi, J. F. Cofactor NAD(P)H regeneration inspired by heterogeneous pathways. *Chem* **2017**, *2*, 621–654.

[12] Mayr, J. C.; Grosch, J. H.; Hartmann, L.; Rosa, L. F. M.; Spiess, A. C.; Harnisch, F. Resting *Escherichia coli* as chassis for microbial electrosynthesis: Production of chiral alcohols. *ChemSusChem* **2019**, *12*, 1631–1634.

[13] Shi, H. L.; Fu, M. R.; Bai, X. Y.; Zhang, X. C.; Li, D. D.; Yao, L. G.; Kan, Y. C.; Xue, C.; Tang, C. D. Improving carbon dioxide conversion efficiency through immobilization of formate dehydrogenase *Pb*FDH and its mutant D533S/E684I on nanostructured carriers. *ACS Sustain. Chem. Eng.* **2025**, *13*, 1271–1280.

[14] Lee, Y. S.; Gerulskis, R.; Minteer, S. D. Advances in electrochemical cofactor regeneration: Enzymatic and non-enzymatic approaches. *Curr. Opin. Biotechnol.* **2022**, *73*, 14–21.

[15] Himiyama, T.; Waki, M.; Maegawa, Y.; Inagaki, S. Cooperative catalysis of an alcohol dehydrogenase and rhodium-modified periodic mesoporous organosilica. *Angew. Chem., Int. Ed.* **2019**, *58*, 9150–9154.

[16] Qiu, S.; Xu, S, Y.; Wang, Y. J.; Zheng, Y. G. Chemoenzymatic catalysis of *tert*-butyl 6-cyano-(3*R*,5*R*)-dihydroxyhexanoate by aldo-keto reductase coupled with composite Fe_3O_4 nanozyme scaffold. *Chem. Eng. Sci.* **2022**, *261*, 117935.

[17] Zhang, L.; Etienne, M.; Vilà, N.; Le, T. X. H.; Kohring, G. W.; Walcarius, A. Electrocatalytic biosynthesis using a Bucky paper functionalized by $[Cp^*Rh(bpy)Cl]^+$ and a renewable enzymatic layer. *ChemCatChem* **2018**, *10*, 4067–4073.

[18] Lee, J. S.; Lee, S. H.; Kim, J.; Park, C. B. Graphene-Rh-complex hydrogels for boosting redox biocatalysis. *J. Mater. Chem. A* **2013**, *1*, 1040–1044.

[19] Sheldon, R. A.; Basso, A.; Brady, D. New frontiers in enzyme immobilisation: Robust biocatalysts for a circular bio-based economy. *Chem. Soc. Rev.* **2021**, *50*, 5850–5862.

[20] Huisman, G. W.; Liang, J.; Krebber, A. Practical chiral alcohol manufacture using ketoreductases. *Curr. Opin. Chem. Biol.* **2010**, *14*, 122–129.

[21] Zhao, H.; Liu, G. H.; Liu, Y. T.; Zhou, L. Y.; Ma, L.; He, Y.; Zheng, X. B.; Gao, J.; Jiang, Y. J. Preparation of hollow spherical covalent organic frameworks via Oswald ripening under ambient conditions for immobilizing enzymes with improved catalytic performance. *Nano Res.* **2023**, *16*, 281–289.

[22] Chambers, M. B.; Wang, X.; Elgrishi, N.; Hendon, C. H.; Walsh, A.; Bonnefoy, J.; Canivet, J.; Quadrelli, E. A.; Farrusseng, D.; Mellot-Draznieks, C. et al. Photocatalytic carbon dioxide reduction with rhodium-based catalysts in solution and heterogenized within metal–organic frameworks. *ChemSusChem* **2015**, *8*, 603–608.

[23] Qin, F. Y.; Qin, B.; Zhang, W. H.; Liu, Y. L.; Su, X.; Zhu, T. H.; Ouyang, J. P.; Guo, J. Y.; Li, Y. X.; Zhang, F. T. et al. Discovery of a switch between prelog and anti-prelog reduction toward halogen-substituted acetophenones in short-chain dehydrogenase/reductases. *ACS Catal.* **2018**, *8*, 6012–6020.

[24] Jiang, Y. Y.; Qu, G.; Sheng, X.; Tong, F. F.; Sun, Z. T. Unraveling the mechanism of enantio-controlling switches of an alcohol dehydrogenase toward sterically small ketone. *Catal. Sci. Technol.* **2022**, *12*, 1777–1787.

[25] Gao, L. Y.; Wang, Z. H.; Liu, Y. T.; Liu, P. B.; Gao, S. Q.; Gao, J.; Jiang, Y. J. Co-immobilization of metal and enzyme into hydrophobic nanopores for highly improved chemoenzymatic asymmetric synthesis. *Chem. Commun.* **2020**, *56*, 13547–13550.

[26] Zhang, W. H.; Carter, B. M.; Day, G. J.; Govan, N.; Jackson, C.; Perriman, A. W. Sequential electrostatic assembly of a polymer surfactant corona increases activity of the phosphotriesterase arPTE. *Bioconjugate Chem.* **2019**, *30*, 2771–2776.

[27] Yan, L. H.; Liu, G. H.; Liu, J. Q.; Bai, J.; Li, Y. X.; Chen, H. X.; Zhou, L. Y.; Gao, J.; Jiang, Y. J. Hierarchically porous metal organic

framework immobilized formate dehydrogenase for enzyme electrocatalytic CO_2 reduction. *Chem. Eng. J.* **2022**, *450*, 138164.
[28] Pace, C. N.; Fu, H. L.; Fryar, K. L.; Landua, J.; Trevino, S. R.; Schell, D.; Thurlkill, R. L.; Imura, S.; Scholtz, J. M.; Gajiwala, K. et al. Contribution of hydrogen bonds to protein stability. *Protein Sci.* **2014**, *23*, 652–661.
[29] Bilal, M.; Cui, J. D.; Iqbal, H. M. N. Tailoring enzyme microenvironment: State-of-the-art strategy to fulfill the quest for efficient bio-catalysis. *Int. J. Biol. Macromol.* **2019**, *130*, 186–196.
[30] Li, L. Y.; Li, Z. X.; Yang, W. J.; Huang, Y. M.; Huang, G.; Guan, Q. Q.; Dong, Y. M.; Lu, J. L.; Yu, S. H.; Jiang, H. L. Integration of Pd nanoparticles with engineered pore walls in MOFs for enhanced catalysis. *Chem* **2021**, *7*, 686–698.
[31] Le, T. X. H.; Charmette, C.; Bechelany, M.; Cretin, M. Facile preparation of porous carbon cathode to eliminate paracetamol in aqueous medium using electro-Fenton system. *Electrochim. Acta* **2016**, *188*, 378–384.
[32] Mahmoud, M.; El-Khatib, K. M. Three-dimensional graphitic mesoporous carbon-doped carbon felt bioanodes enables high electric current production in microbial fuel cells. *Int. J. Hydrogen Energy* **2020**, *45*, 32413–32422.
[33] Cui, H. F.; Du, L.; Guo, P. B.; Zhu, B.; Luong, J. H. T. Controlled modification of carbon nanotubes and polyaniline on macroporous graphite felt for high-performance microbial fuel cell anode. *J. Power Sources* **2015**, *283*, 46–53.
[34] Hollmann, F.; Schmid, A.; Steckhan, E. The first synthetic application of a monooxygenase employing indirect electrochemical NADH regeneration. *Angew. Chem., Int. Ed.* **2001**, *40*, 169–171.
[35] Kim, S.; Kim, M. K.; Lee, S. H.; Yoon, S.; Jung, K. D. Conversion of CO_2 to formate in an electroenzymatic cell using *Candida boidinii* formate dehydrogenase. *J. Mol. Catal. B: Enzym.* **2014**, *102*, 9–15.
[36] Zhang, L.; Vilà, N.; Kohring, G. W.; Walcarius, A.; Etienne, M. Covalent immobilization of (2,2'-bipyridyl) (pentamethylcyclopentadienyl)-rhodium complex on a porous carbon electrode for efficient electrocatalytic NADH regeneration. *ACS Catal.* **2017**, *7*, 4386–4394.
[37] Hollmann, F.; Arends, I. W. C. E.; Buehler, K. Biocatalytic redox reactions for organic synthesis: Nonconventional regeneration methods. *ChemCatChem* **2010**, *2*, 762–782.
[38] Liu, G. H.; Chen, H. X.; Zhao, H.; Chen, R.; Yang, M. H.; Gao, J.; Yu, F. S.; Jiang, Y. J. Accelerating electroenzymatic CO_2 reduction by immobilizing formate dehydrogenase on polyethylenimine-modified mesoporous silica. *ACS Sustain. Chem. Eng.* **2022**, *10*, 633–644.
[39] Liu, G. H.; Wang, L. R.; Yan, L. H.; Zhao, H.; Li, Y. X.; Zhou, L. Y.; He, Y.; Ma, L.; Liu, Y. T.; Gao, J. et al. A dual-enzyme microreactor based on encapsulation and covalent bond for enzymatic electrocatalytic CO_2 reduction. *Chem. Eng. J.* **2023**, *475*, 146186.
[40] Cheng, Y. Q.; Shi, J. F.; Wu, Y. Z.; Wang, X. Y.; Sun, Y. Y.; Cai, Z. Y.; Chen, Y.; Jiang, Z. Y. Intensifying electron utilization by surface-anchored Rh complex for enhanced nicotinamide cofactor regeneration and photoenzymatic CO_2 reduction. *Research* **2021**, *2021*, 8175709.
[41] Yang, D.; Zhang, Y. S.; Zou, H. J.; Zhang, S. H.; Wu, Y. Z.; Cai, Z. Y.; Shi, J. F.; Jiang, Z. Y. Phosphorus quantum dots-facilitated enrichment of electrons on g-C_3N_4 hollow tubes for visible-light-driven nicotinamide adenine dinucleotide regeneration. *ACS Sustain. Chem. Eng.* **2019**, *7*, 285–295.
[42] Wu, Y. Z.; Ward-Bond, J.; Li, D. L.; Zhang, S. H.; Shi, J. F.; Jiang, Z. Y. g-C_3N_4@α-Fe_2O_3/C photocatalysts: Synergistically intensified charge generation and charge transfer for NADH regeneration. *ACS Catal.* **2018**, *8*, 5664–5674.
[43] Liu, Y. T.; Yan, J. J.; Yuan, Q.; Ma, L.; Zhou, L. Y.; He, Y.; Liu, G. H.; Yue, X. Y.; Jiang, Y. J. Enzymatic reduction of halogenated aryl ketones in an aqueous micellar solution with enhanced catalytic performance. *Green Chem.* **2024**, *26*, 6666–6674.